

Multielectron excitations in x-ray absorption spectra of Rb and Kr

A Kodre^{1,2}, I Arčon^{2,3}, J Padežnik Gomilšek⁴, R Prešeren¹ and R Frahm⁵

¹ Faculty of Mathematics and Physics, University of Ljubljana, Jadranska 19, SI-1000 Ljubljana, Slovenia

² J Stefan Institute, Jamova 39, PP 3000, SI-1001 Ljubljana, Slovenia

³ Nova Gorica Polytechnics, Vipavska 13, PO Box 301, SI-5001 Nova Gorica, Slovenia

⁴ Faculty of Mechanical Engineering, University of Maribor, Smetanova 17, SI-2000 Maribor, Slovenia

⁵ Bergische Universität Gesamthochschule Wuppertal, Fachbereich 8-Physik, Gaußstraße 20, D-42097 Wuppertal, Germany

E-mail: alozj.kodre@fmf.uni-lj.si

Received 5 February 2002, in final form 30 May 2002

Published 12 August 2002

Online at stacks.iop.org/JPhysB/35/3497

Abstract

In the K-edge x-ray absorption of rubidium vapour and gaseous krypton, comprehensive spectra of collective excitations down to the relative probability of 5×10^{-5} are extracted. After removal of the asymptotic Victoreen trend, the region ~ 100 eV above the edge exhibits a steep decrease of the absorption coefficient attributed to core relaxation and post-collision interaction in the Auger decay. With an exponential model for the decrease, the entire spectrum of multielectron excitations is recognized as a succession of consecutive resonant, shake-up and shake-off channels. They can be identified as coexcitations of electrons from successively deeper subshells, from 5s down to 3s.

The identification of excited states is aided by a quantitative modelling of subshell contributions and by natural-width deconvolution. The valence and subvalence coexcitations are shown to follow the pattern of the lighter homologues potassium and argon.

1. Introduction

Absorption spectrometry, the simplest spectroscopic technique in the x-ray field, has contributed important information on the detailed structure of the atomic system. The data it provides is simply proportional to the transition probability, almost without interference with instrumental effects, so that even a conversion to the absolute cross section is highly reliable. However, the technique provides only the total cross section: to distinguish between contributions of separate reaction channels, other techniques, e.g. emission spectroscopies, are required. In the study of multielectron photoexcitation (MPE), a process which may

probe directly the correlation in the motion of electrons, synchrotron measurements of x-ray absorption on noble gases have provided spectra with high sensitivity and practically lifetime-width resolution [1–12]. The MPE channels in these spectra are recognized by sharp threshold features superposed onto the smooth energy dependence of the dominant channel of the single-electron photoeffect. Tiny resonant peaks and absorption edges are identified as signatures of double excitations and shake-up transitions, respectively. In high quality spectra, a shake-off transition or double ionization can be recognized as a change of slope at the threshold [8]. Superposition of reaction channels can give rise to more complex spectral features [13].

In addition to characteristic shape, the threshold energy is the key for identification of the MPE channels: mostly, experimental data are compared with SCF (self-consistent field) energy estimates of candidate excited states. For a definite assignment of MPE features, especially in complex cases, a reconstruction of the experimental cross section by a theoretical model is required. Good results have been obtained for some isolated groups of excitations in noble gas spectra [8, 14–18]. The theoretical treatment, however, has been uniquely adapted to each case, allowing little generalization. An *ab initio* calculation of the full range of MPE is still beyond the reach of the models. In the absence of theoretical data the interpretation of MPE spectra can be aided by inclusion of additional experimental data, e.g. emission spectra [1, 19–21]. The gradual evolution of spectral features in related systems, such as isoelectronic series of ions [22–29], can be used to the same effect. In particular, the comparison of richly detailed MPE spectra of the neighbours argon and potassium [27] provided insight into specifics of their electronic structure.

In the present study, the atomic absorption of rubidium is compared to that of the neighbour noble gas krypton. The Rb data for the study are taken from a series of measurements on a Rb vapour cell [30]. The absorption spectrum of the monatomic metal vapour is free of the structural signal (XAFS) so that pure MPE features are recovered in detail comparable to that in the spectra of noble gases. The spectra in the series have been obtained over a longer period in experimental runs at different synchrotron beamlines, with improving energy resolution and signal-to-noise ratio stemming from improvements in the cell design and monochromator characteristics. Although the latest (and best) data will be used in the presentation, the consistency of the entire series provides a guarantee against contamination of the MPE data with monochromator artifacts.

The MPE spectrum of krypton has been extensively studied [3–8]. It has served as a test case for several new approaches in the analysis. Schaphorst *et al* [8] built a quantitative MPE model of the major excitation channels resolved in the modest sensitivity of the experiment. The improved resolution and sensitivity in the experiment by Filipponi opened the way to the technique of natural-width deconvolution [34]. The Kr data, analysed in the present report, were remeasured at the same experimental station.

From the earlier data in the Rb series the XAFS atomic absorption background of Rb has been constructed [31, 32], and, with an additional normalization measurement, the absolute Rb photoabsorption cross section too [33]. In the present paper, a comprehensive explanation of the absorption spectrum is given on the basis of the energy levels of single and multiple excitations of the Rb and Kr atoms. Energy estimates from Hartree–Fock (HF) and Dirac–Fock (DF) self-consistent atomic models, including the effect of configuration interaction (CI), are used in identification of MPE features. In the parallel analysis of Kr and Rb we exploit the fact that the cores of the two atoms are largely the same, apart from the unit difference in the nuclear charge, and rubidium has an additional loosely bound electron in the 5s shell. It is shown how the common features in the spectra follow from a specific interaction of core configurations, while the differences in the MPE features stem from the additional coupling of the Rb 5s electron and the collapse of the 4d orbital in some excited states of Rb.

Instead of a reconstruction of the MPE cross section *ab initio*, which requires a much more potent theoretical apparatus, our quantum mechanical explanation of the MPE features is based on a full scale modelling. With sufficient quality of spectra available on the latest generation of synchrotron x-ray sources the spectral features can be modelled quantitatively by linear combinations of theoretical energy profiles of reaction channels. The identification of the features is thus transferred to the much more transparent manifold of model parameters where *a priori* physical constraints (energy splitting, intensity ratios, widths) can be easily taken into account or even introduced into the modelling step. The basic tenet of the approach is that with sufficiently low level of noise even the features that are lost from view due to a low amplitude or a large width leave a mark deeper in the dynamical range of the bin count and can, consequently, be recovered numerically.

In the related technique of natural width deconvolution [34] the identification of spectral features is facilitated by suppression of the linewidth in a numerical transformation without a specific model. It has been shown in some earlier attempts [35–37] that the energy resolution of spectral features can be improved at the expense of signal-to-noise ratio. Filipponi [34] has published a general purpose algorithm, implemented in a computer program, by which the entire natural width can be removed and substituted by a considerably smaller Gaussian width. Although the deconvolution can always be simulated after a successful modelling, its advantages are the immediate visualization and applicability to cases where a model is not evident.

The success of both techniques, however, depends critically on the signal-to-noise ratio. Even with the brightness of modern synchrotron x-ray sources a sufficiently low noise is hardly achieved in a single scan: averaging over several identical scans to suppress noise is usually required for a meaningful exploitation of either technique.

2. Experiment

Absorption spectra of krypton and rubidium vapour in the K-edge region were measured at the X1 station of HASYLAB at Deutschen Elektronen-Synchrotron (DESY, Hamburg, Germany), and at beamline BM29 of the ESRF in Grenoble, France. Fixed-exit Si(311) double-crystal monochromators were used, with FWHM resolution of 2 and 1 eV, respectively, at 15 keV. The values were chosen above the monochromator geometrical limit to retain the intensity: the sharpness of the spectral features could hardly be improved by additional decrease of experimental width in view of the ~ 3 eV natural width. The harmonic components of the beam were suppressed by detuning the monochromator to the 60% point of the rocking curve. The flux of the incident monochromatic x-ray beam and the flux of the transmitted beam through the sample were measured by ionization detectors filled with argon.

An atomic Rb sample was prepared in a metal-vapour cell constructed to contain dense vapour with the absorption length of the order of unity [30]. By monitoring the absorption in the cell as a function of the temperature, the working point was chosen slightly above the temperature where the metal was completely vapourized (vapour pressure 71.3 kPa at 690 °C), to stabilize the sample density. The Kr gas sample was contained in a glass cell sealed by kapton windows with Kr absorption thickness of unity above the K edge. The energy scale of the monochromator was calibrated with the features of the Kr K edge [38]. The reproducibility of the energy scale in Rb absorption scans was established with a parallel measurement of the Pb L₂ edge (15 200 eV). The contributions of the window absorption and of the energy-dependent detector efficiency were exactly determined in a reference measurement *in situ*, by removing the gas from the beam path, either by evacuating (Kr) or by cooling the cell (Rb).

The absorption coefficient for Kr and Rb in the energy region above the K edge is shown (figure 1) as a superposition of five and 15 experimental runs, respectively. The features seen

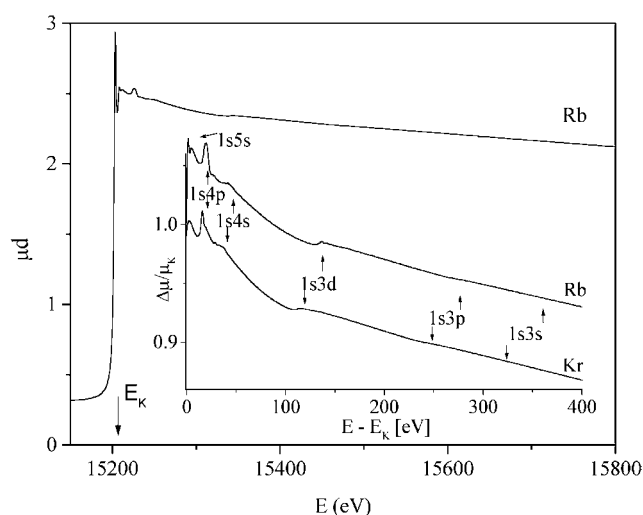


Figure 1. Absorption spectrum of Rb in the vicinity of the K edge (15 206.9 eV). Inset: normalized above-edge spectra of Rb and Kr in the relative energy scale. DF estimates of thresholds of coexcitation groups are indicated.

in the two spectra are remarkably similar. Common to both are a group of resonances within 60 eV above the K edge and two points of discontinuity of slope (140 and 280 eV in Rb). Using DF [39] estimates of excitation energies, the features are attributed to coexcitations of electrons from consecutive subshells. Apart from these sharp features, the region from the K edge to the 3d group exhibits a steeper slope than the region further out. Thus, the photoabsorption cross section immediately above an inner-shell edge is larger than the value extrapolated from the asymptotic trend. The observation, found in all noble-gas experiments, has been explained as a contribution of core relaxation (CR) and post-collision interaction (PCI) in Auger decay of the core hole [40, 41].

3. Analysis

The MPE features in the absorption spectra of Kr and Rb will be discussed following the order of the well separated groups of coexcitations of consecutive subshells. The introductory analysis of the K edge reveals some details of CI and coupling useful in explanation of the weaker subshell MPE features. The region of the steeper slope is discussed separately. The model of the CR/PCI contribution extending over the entire MPE spectrum is described with a heuristic ansatz to provide a clearer view of the MPE.

Both deconvolution and comprehensive modelling of the features are used to sharpen the detail and to facilitate the identification of excitation channels. The model decomposition of features is shown in the simpler cases of deep MPE, while for the complex subvalence MPE (1s5s, 1s4p and 1s4s) the deconvoluted picture provides better insight.

In modelling, the MPE features are reconstructed by a superposition of three types of functional component: Lorentzian peaks

$$A \left[\frac{\Gamma^2}{4(E - E_0)^2 + \Gamma^2} \right]$$

for resonant channels, cumulative Lorentzian distribution

$$A \left[\frac{1}{2} + \frac{1}{\pi} \operatorname{arctg} \left(\frac{E - E_0}{\frac{\Gamma}{2}} \right) \right]$$

for shake-up edges and exponential saturation profiles

$$A \left[1 - \exp \left(-\frac{E - E_0}{\Gamma} \right) \right] \quad \{E > E_0\}$$

for shake-off channels.

The first two are characterized by three standard parameters, the amplitude A , the width Γ and the energy E_0 . In exponential saturation, the energy parameter is the threshold of the shake-off channel, and the width is given by the range, i.e. the reciprocal of the saturation constant. For resonant lines, the intensity will be given as the product of the amplitude and the width so that a comparison between groups and elements is enabled.

For the shake-off channel another theoretical ansatz (Thomas profile) has been derived from a statistical description of the process [20]. The comparison with satellite emission data on Cu [19] shows that an exponential saturation profile can be adapted to a closer fit. Since this functional form also follows from the statistical description with a slightly different yet entirely physical assumption on the momentum density we adopt it in the present study. The range of the exponential is proportional with the excess energy, i.e. the binding energy of the shaken electron. The coefficient of proportionality in Cu data is 0.4, and the same value will be used here, in satisfactory agreement with the data.

3.1. K edge

The deconvolution is best exploited in the region of major absorption edges where the obscuring effect of strong and extensive tails of the edge and the accompanying resonance lines is removed and finer features become visible. In Kr and Rb, the deconvoluted K-edge regions appear almost identical to those of the lighter homologues Ar and K (figures 2(a) and (b)) when intensity relative to the K-edge jump is considered and the energy scale relative to the K edge is used. The span of edge features in Rb and Kr appears slightly contracted since the excited states are less tightly bound due to a weaker penetration of outer electrons to the core.

The simple edge shape of Kr can be modelled with just three elements (table 1), the resonant peak of the [1s]5p transition, its Rydberg follower [1s]6p and the K edge [1s] itself. The position of the model edge is shifted from the DF estimate by 0.7 eV, owing to the accumulation of unresolved lines of the Rydberg series [42].

In Rb, considerable additional detail is introduced by the presence of the valence 5s electron (table 1). As in the case of potassium, the DF calculation shows that in the resonant [1s]5p state the coupling is pure (5s5p)1s, leading to a triplet–singlet splitting of 1.9 eV. CI suppresses the splitting; the definite value is not known for convergence problems in the DF code. The extrapolation from DF models with artificially increased nuclear charge points to a value of 1.4 eV, obtained at $Z_{eff} = 37.15$. The least-squares value from experimental data is 1 ± 0.3 eV, with the intensity ratio of the two components of 4.8:1.

The coexcitations of the 5s valence electron follow immediately above the [1s] edge. The resonant peak due to the [1s5s]5p6s transition is plainly visible in the measured spectrum. The deconvolution also reveals the Rydberg resonance [1s5s]6p6s and the shake-up edges [1s5s]5p and [1s5s]6s. The latter, stemming from the ordinary shake promotion of the valence electron in the 1s photoeffect, appears stronger than the reverse possibility of the valence monopole ejection accompanying a dipole $1s \rightarrow 5p$ excitation.

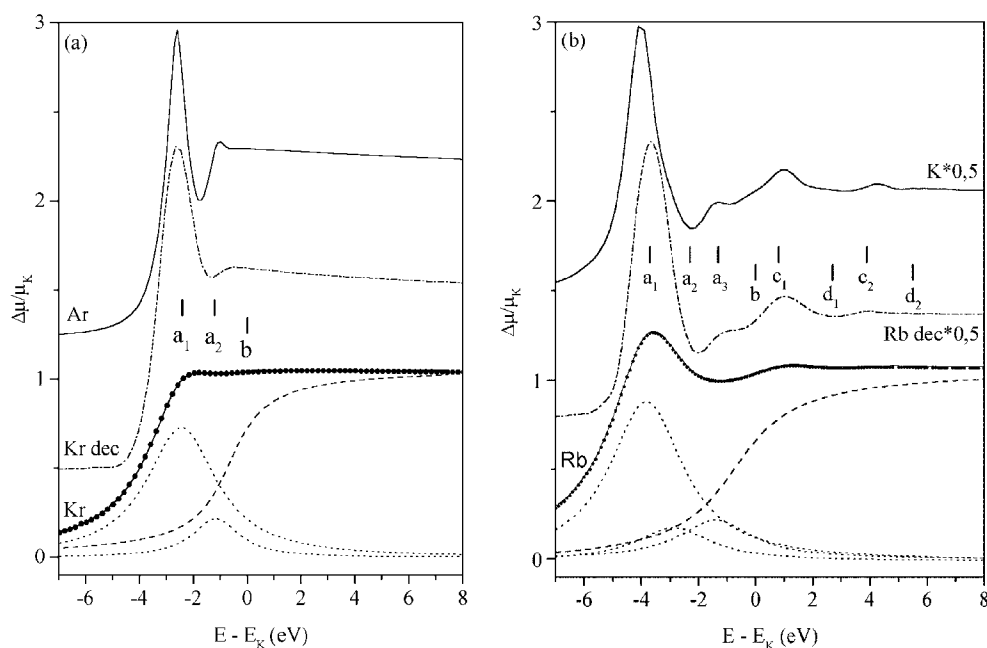


Figure 2. Normalized Kr and Rb K edge (solid) and some of the model components (dashes, dots)—see table 1. The deconvoluted spectra (dash-dots) are compared, respectively, to argon and potassium K edges (above). DF energies are indicated. Energy scale here and subsequently as explained in table 1.

3.2. Core relaxation and PCI

If quantitative agreement with experimental data is required even the theoretical reconstruction of the dominant single-electron photoabsorption channel without MPE contributions represents a difficult task, as shown in the analyses of the Kr K edge [5, 8]. The asymptotic decrease of the photoelectric cross section far above the edge can be described sufficiently well by a Victoreen power formula E^{-n} , n around 3, but for the region of steeper slope immediately above the edge a quantitative model has not yet been given. In figure 1, the region seems to reach as far as the 1s3d MPE group. According to Tulkki and Aberg [40], the cross section calculated with inclusion of CR and PCI effects exceeds the unrelaxed cross section immediately above the edge but approaches it asymptotically. The contribution of the relaxation and PCI may thus be regarded as superposed onto the single electron cross section. Its overall effect in the Kr absorption spectrum has already been discussed by Deutsch *et al* [5, 11].

The presence of the CR/PCI contribution affects the definition of the edge amplitude. To maintain the consistency with tabulated absorption data we define the amplitude of the edge as the Victoreen extrapolation from values far above the edge. It is thus the photoabsorption cross section with saturated shake channels, extrapolated to the edge energy. The extrapolation, however, excludes the CR/PCI contribution since it dies out before the asymptotic region.

In analysis of MPE groups it proves useful to eliminate the Victoreen trend from the measured absorption spectrum since its slope affects the shapes of weaker MPE details. Following the above discussion, we divide the experimental cross section by the Victoreen cross section, determined in a least-squares fit in the high-energy region above perceptible MPE features. The renormalized spectrum is seen as a slow decrease, interspersed with sharp MPE features, from the K edge to the asymptotic unit value (figure 3(a)).

Table 1. Best-fit model parameters of the normalized Kr and Rb K edges and calculated DF energies of the corresponding electron transitions relative to the $1s \rightarrow \varepsilon p$ threshold ($E_K = 14\,326.4$ and $15\,205.6$ eV respectively). The respective experimental values $14\,327.0$ and $15\,206.9$ eV are established from the positions of the pre-edge resonant peaks. The apparent edge in the spectrum is shifted downwards by the accumulation of unresolved lines of the Rydberg series. A common value for the linewidths of the model elements is 3.1 eV.

Kr	Label	Model		DF
		$E - E_K$ (eV)	$A\Gamma$ (eV)	$E - E_K$ (eV)
[1s]5p	a ₁	-2.4	2.3	-2.4
[1s]6p	a ₂	-1.2	0.5	-1.2
[1s]	b			0
Edge		-0.7		
Rb				
[1s]5p triplet	a ₁	-3.8	2.8	-3.7
[1s]5p singlet	a ₂	-2.8	0.6	-2.3 ^a
[1s]6p	a ₃	-1.4	0.7	-1.3
[1s]	b			0
Edge		-0.7		
[1s5s]6s5p	c ₁	0.9	0.2	0.8
[1s5s]5p	d ₁			2.7
[1s5s]6s6p	c ₂	4.8	0.05	3.9
[1s5s]6s	d ₂			5.5
[1s5s]				10.4

^a At increased nuclear charge $Z = 37.15$ (see text).

Table 2. Range of the exponential ansatz for some elements. The numbers in brackets indicate the uncertainty of the last digit.

Element	Ar	Ge	Se	Kr	Rb
Range (eV)	8(2)	16(4)	20(8)	43(9)	45(8)

The smooth segments of the spectrum between MPE groups look like parts of a single continuum with steadily decreasing slope. In an attempt to describe the continuum with a simple function of energy, an exponential is found to fit surprisingly well. Indeed, the exponential determined to fit the most conspicuous smooth spectral region between $1s4s$ and $1s3d$ MPE groups also remains roughly parallel with the flat segments on either side. Its removal results in a *reduced cross section* (figure 3(b)) that increases stepwise to the asymptotic value of 1. The monotonic increase, if the narrow resonant contributions are momentarily disregarded, follows from the succession of the shake-up and shake-off channels. Several ambiguous MPE features, e.g. sharp spikes of the $1s4p$ group, can now be clearly identified: after removing additional slope the resonant and shake-up channels are easily discerned. Likewise, the saturation profile of shake-off channels is made evident.

The same procedure is successful for Rb. The reduced cross sections of figure 3(b) will be used in the analysis of MPE in Kr and Rb, and the channel strengths will refer to the particular renormalization discussed above. The exponential *ansatz*, however heuristic and approximate, also applies in other similar cases, as in the high-resolution absorption spectra of hydrides of the 4p elements [43]. Even the 20 eV long stretch of smooth cross section between the edge and the valence MPE group ($1s3p$) in the spectra of Ar and K [27] fits an exponential well. The effective range of the exponential shows a distinct increase with atomic number Z (table 2).

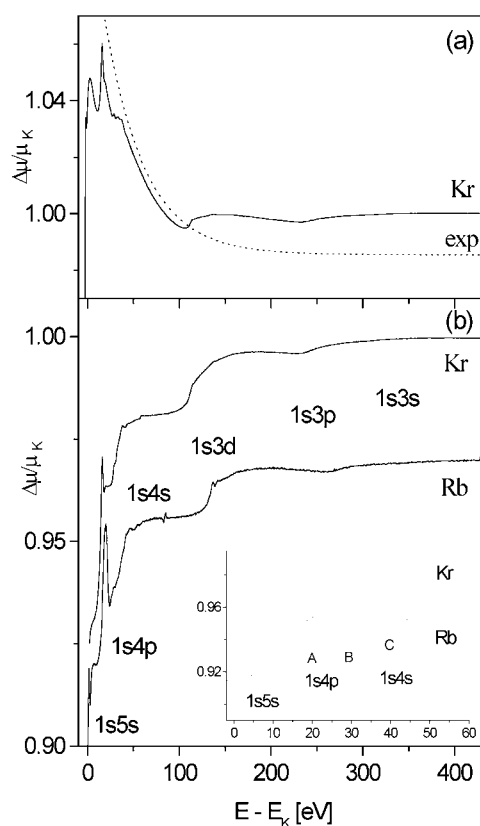


Figure 3. (a) Kr absorption cross section normalized to the asymptotic Victoreen formula; an arbitrarily shifted exponential ansatz for PCI contribution; (b) reduced MPE spectrum of Kr and Rb after removal of the best-fit exponential. The inset shows an expanded view of the complex region just above the edge with 1s5s, 1s4p and 1s4s excitations. Labels A–C are discussed in the text.

3.3. 1s4p and 1s4s excitations

After the removal of the exponential ansatz the prominent spectral feature in the interval between 10 and 50 eV above the K edge is disclosed as a resonance and an edge in close succession and a compound edge further out (inset in figure 3(b)). The energies are in rough agreement with DF estimates for [1s4p] and [1s4s] states. In Rb, the resonance (A) is considerably wider than in Kr, more than expected from the slight increase of the K vacancy lifetime width (2.75 eV in Kr, 2.99 eV in Rb [44]). Conversely, the adjacent edge (B) is higher in Kr. The compound [1s4s] edge (C) appears similar in both elements.

The picture becomes considerably clearer in the deconvoluted spectrum of Kr (figure 4(a)) where the striking similarity with Ar is demonstrated. The same series of channels can be followed in both elements: a Fano resonance (a_0), a sharp resonance ($a_{1,2}$) and a subsequent edge (a_3), a [1s4s] resonance (b_1) and the edge (b_2) with superposed diffuse structure.

In Rb (figure 4(b)), only a part of the natural width may be removed by deconvolution due to a higher level of noise, so most of the detail remains hidden. The wide [1s4p] resonance reveals a composite structure, comparable to that in the homologue K. The strength of the resonant channel is larger than in Kr by a factor of 1.4: this value is close to the corresponding

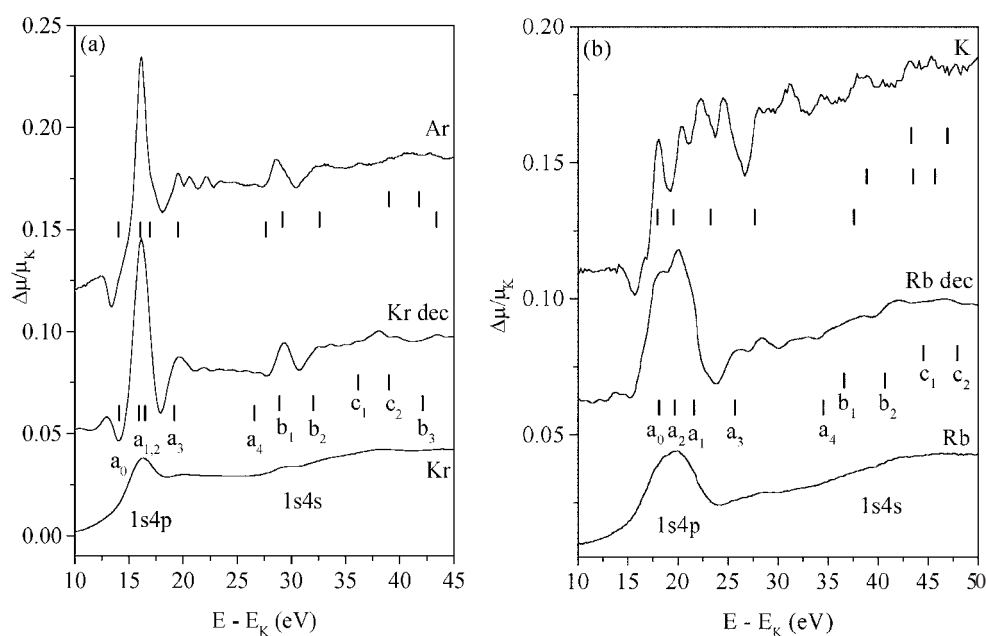


Figure 4. Details of 1s4p and 1s4s MPE groups in Kr and Rb (below). Note the similarity of the deconvoluted spectra (middle) with the respective Ar and K 1s3p groups (above). Corrected HF excitation energies (see text) and labels in table 3. The Ar and K data are shifted by 3.2 and 3.8 eV, respectively.

Table 3. Corrected HF energies (see text) of 4p and 4s coexcitations in Kr and Rb.

Transition	Label	Kr	Rb
		$E - E_K$ (eV)	$E - E_K$ (eV)
[1s4p]4d5s	a_0	14.1	18.1
[1s4p]5p ²	a_1	15.9	21.6
[1s4p]4d ²	a_2	16.5	19.7
[1s4p]5p	a_3	19.2	25.7
[1s4p]	a_4	26.6	34.5
[1s4s]5s5p + [1s4p ²]4d5s5p	b_1	28.9	36.6
[1s4s]5s + [1s4p ²]4d5s	b_2	32.0	40.7
[1s4s] + [1s4p ²]4d	b_3	42.1	51.9
[1s4p ²]4d ² 5p	c_1	36.2	44.5
[1s4p ²]4d ²	c_2	39.0	47.9

factor of 1.5 for the 1s \rightarrow 5p single-electron resonances at the K edge. The subsequent [1s4p] edge is smaller in Rb by a factor of 1.7.

The energy markers (a–c) in figures 4(a) and (b) are obtained in a combined HF–DF calculation where average multiplet energies from HF [45] are corrected for the CI shifts from DF. The complete analogy with Ar and K provides the candidate coupling scheme and CI in the initial and final states [16, 17, 27]. The prominent resonance is a combination of [1s4p]5p² and [1s4p]4d² states (a_1 and a_2 , respectively), the latter accessible from the admixture of the [4p²]4d² ground state by a single electron transition 1s \rightarrow 4p. In Kr, the two mixing multiplets occupy the same narrow energy interval and form a sharp resonant peak. In Rb, the HF centre

of gravity for $5p^2$ lies almost 2 eV higher, and the resulting compound resonance is accordingly wider. The subsequent edge (a_3) is predominantly of $[1s4p]5p$ character—it is the Rydberg limit of the $[1s4p]5p^2$ component of the mixed $a_{1,2}$ resonance. The other component has a Rydberg daughter $[1s4p^2]4d^25p$ at c_1 and the continuum limit $[1s4p^2]4d^2$ at c_2 .

The Fano resonance a_0 at the low-energy side of the feature is a fingerprint of the interaction of the Rydberg d series and continuum d states admixed to the 4d orbital in the weak $[1s4p]5s4d$ transition.

In explanation of the $[1s4s]$ resonance (b_1), the agreement between the experiment and the DF estimates is obtained after admixing of appropriate $[1s4p^2]$ excitations, as already demonstrated by Dyllal [46] for the case of the Ar $[1s3s]$ feature. There, the mixing provided the necessary 5 eV shift of the $1s3s$ resonant state. In Kr and Rb, the calculation of the analogous mixing of $[1s4s]5p5s$ and $[1s4p^2]5s5p4d$ states does not converge: the extrapolation of results from a series of atoms with augmented Z values gives a shift of -4.5 eV. The mixing ratio 2:1 is roughly the same as the 68:32 ratio reported for Ar. With a similar calculation, the subsequent edge is recognized as a mixed $[1s4s]5s + [1s4p^2]5s4d$ state (b_2), i.e. the promotion of the 1s electron to a continuum p state, with the same coexcitation(s) as in the resonance.

The definite presence of the $5s4d$ combination precludes the attractive idea that the strong b_1 peak and the subsequent b_2 edge result from another instance of a direct excitation from the ground state admixture $[4p^2]4d^2$, namely by a single electron transition $1s \rightarrow 5p$ or $1s \rightarrow \epsilon p$. As already mentioned, their fingerprints are the resonance c_1 and the edge c_2 which lie considerably higher and do not mix with the $[1s4s]5p5s$ or $[1s4s]5s$ state. However, the double vacancy $[4p^2]$ in the ground-state admixture $[4p^2]4d^2$ as well as in the triple excitation $[1s4p^2]5s4d np$ is 1D , and so are both promoted pairs $4d^2$ and $5s4d$, respectively.

3.4. $[1s3d]$ excitations

The relatively strong $[1s3d]$ MPE group shows, on a finer scale, a lot of detail modifying the basic shake profile (figure 5). The profile includes a distinct shake-off component recognizable by its slow saturation. Its total amplitude is approximately equal to the shake-up edge amplitude, although the latter saturates in the span of the natural width (a few electronvolts) and the former in the range of the order of MPE excitation energy, i.e. the binding energy of the coexcited 3d electron (50 and 60 eV in our shake-off model, for Kr and Rb, respectively).

The leading resonance in the d coexcitation has been shown to maintain a fixed ratio to the K-edge resonance: the relation has been followed in the 4d MPE features from xenon far into the lanthanide series [22, 24, 25]. The $1s3d$ resonances in Kr and Rb in figure 5 also seem to keep the relation of the respective resonant $1s \rightarrow 5p$ excitations at the K-edge. The observation is supported by the absorption spectrum of Rb^+ ion in an aqueous solution of $RbNO_3$ [31, 47]. There, the 3d peak is stronger and wider than the 3d peak in the Rb vapour spectrum, in the same way as the prominent $1s \rightarrow 5p$ white line in the ion spectrum is stronger and wider than the Rb vapour $1s \rightarrow 5p$ resonance. The empirical finding may have a simple explanation: if the core excitation ($1s \rightarrow np$) and the coexcitation ($d \rightarrow d$) do not involve the same orbitals, the transition matrix element factorizes (to a good approximation) so that the strength of the coexcitation follows the strength of the single-electron excitation at the edge.

The Rb spectrum provides an additional puzzle: the $1s3d$ resonance is recognizably split. The splitting of 6 eV, however, does not readily suggest what states might be involved: the $3d_{3/2}-3d_{5/2}$ splitting is much smaller. The analysis of the $[1s3d]5p4d$ multiplet with the total spread of 9.1 eV shows a dense group between 0 and 4.5 eV, and two separate levels, at 7.2 and 9.1 eV in almost pure LS coupling of $[3d]4d^1S$. The direct promotion of the d electron may give these levels a larger cross section, so that they show up in comparable strength to

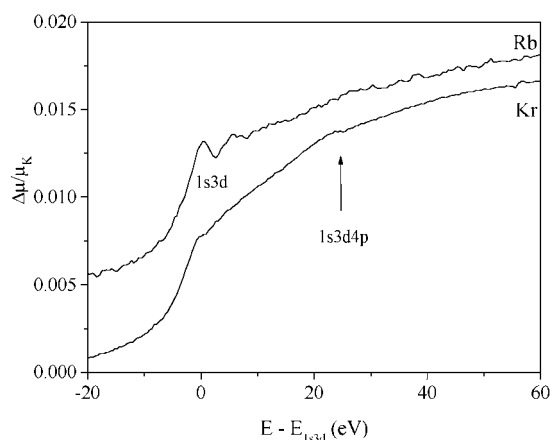


Figure 5. 3d coexcitations in Rb and Kr. The origin of the energy scale is shifted to the position of the leading 1s3d peak. The position of the triple 1s3d4p excitation is indicated.

the large group below 4.5 eV where all levels involve d promotion with a nonzero change of angular momentum.

In Kr, the spread of the multiplet is only one half that of Rb, with the two direct-promotion levels at 4.6 and 4.7 eV. The effective width of the group is thus below 3.5 eV, forming a single peak in the 3 eV natural width spectrum. The observed difference in the widths of the multiplet between the two elements can thus be ascribed to the imminent collapse of the 4d orbital: Rb[1s3d] with two core vacancies is already on the other side of the collapse threshold. The shake-up multiplets [1s3d]4d show analogous splitting to the respective resonant multiplets. In the shake-off multiplets [1s3d], which involve no 4d orbital, there is a single tight group of levels.

The flat rise of the cross section above the resonance in both elements is a superposition of the shake-off profile and a small hump 25 eV above the 3d threshold. In Kr, the hump has been ascribed to a triple vacancy state [7] without identification of reaction channels. Figure 6 shows the sum of two-electron excitation components of our model: the residual in Kr resembles the profile of the 1s4p/4s group. It comprises a resonance and an edge, with energies close to the [1s3d4p]4d³ and [1s3d4p]4d², respectively, and possibly a shake-off component. The similarity with the 1s4p/4s group is apparent also in Rb, in spite of larger noise level. The unusual strength of the triple excitation can again be explained as a transition from the [4p²]4d² component of the ground state whence two electrons are promoted: 1s → 4p accompanied by either 3d → 4d or 3d → εd. In the sharper Kr spectrum, the removal of the double-vacancy components from the 1s3d feature even reveals a tiny Rydberg daughter 1s → 5p belonging, formally, to a quadruple vacancy state [1s3d4p²]!

3.5. [1s3p] and [1s3s] excitations

The 1s3p feature is recognized as a distinct break of slope 240 and 270 eV above the K edge of Kr and Rb, respectively, close to the DF energy estimates. Pure contribution of the [1s3p] channels is revealed after a careful elimination of the [1s3d] shake-off upon which it is superposed. The long saturation profile points to a predominant shake-off character. Yet the vestiges of a structure immediately above the threshold also reliably define a resonant and a shake-up contribution, both in a doublet with a splitting of approximately 8.5 and 10 eV for Kr and Rb,

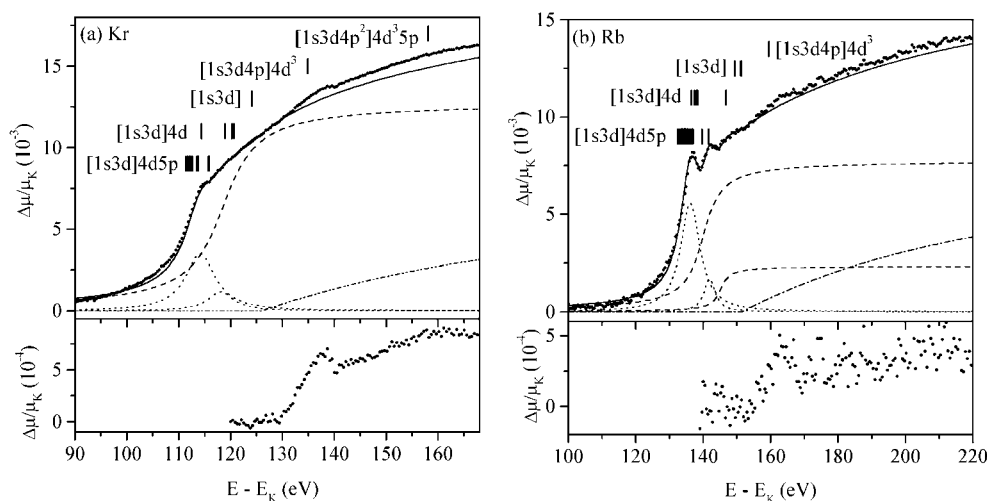


Figure 6. Model components of the Kr and Rb 1s3d group: resonant (dots), shake-up (dashes) and shake-off (dash-dots) two-electron channels. The residual (below) indicates the presence of tri- and perhaps even four-electron excitations. DF multiplets and HF levels are shown. Note the similarity of the residuals to the respective 1s4p structures in figure 4.

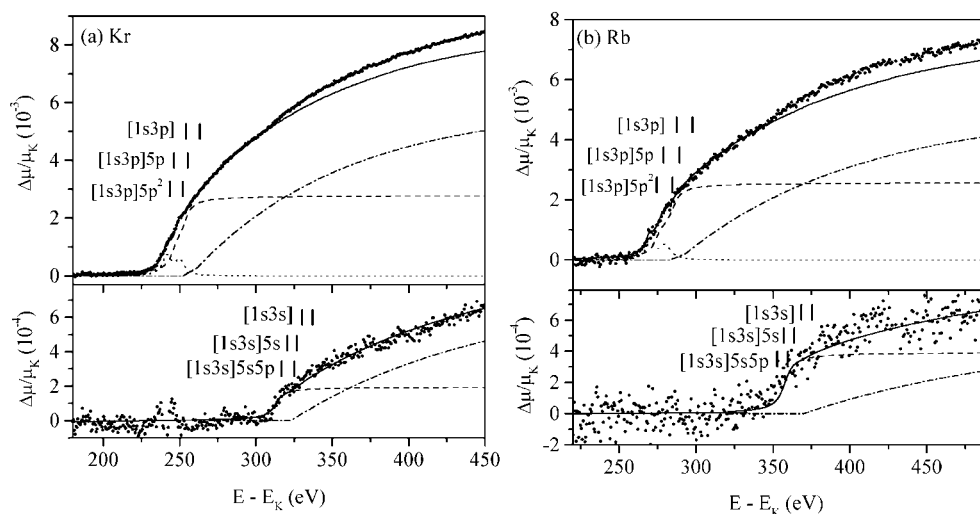


Figure 7. Model components of the 1s3p and 1s3s groups in Kr and Rb. Channels of the 1s3p group are subtracted to show the 1s3s group as a residual. It is only decomposed into a single shake-up and shake-off component due to the large noise.

respectively (figure 7). The splitting is induced by the $3p_{1/2}$ – $3p_{3/2}$ subshell structure which remains the main feature of the multiplets in spite of coupling with 1s and excitation orbitals.

A small [1s3s] feature can be resolved in the residue after subtraction of the [1s3p] model components from the experimental spectrum. The feature in Kr is revealed as a small and broad absorption edge close to the energy of the DF estimate. A similar edge is recognized in Rb in spite of larger noise. This is the deepest MPE observed so far. As in the case of [1s3p], the feature is a combination of a [1s3s] shake-up and shake-off channel. The large

width is partly due to the 6 eV singlet–triplet splitting of the [1s3s] vacancy pair, and partly due to the intrinsic lifetime width, the sum of the [1s] and [3s] widths. The model amplitude of the shake-off transition is strongly coupled with the parameters of the [1s3p] shake-off upon which the feature is superposed.

Among earlier discussions of the Kr MPE spectrum, Deutsch and Hart [3, 4] identified all subshell groups and their main features. The [1s3s] feature in their report [3] appears within 5 eV of ours. The estimated amplitudes of the shake-up and shake-off exceed ours by a factor of two.

4. Discussion and results

The deep MPE from the 1s3d group on can be well described by relatively simple model combinations of a resonant, a shake-up and a shake-off term. As shown in table 4, pairs of terms are often included to model multiplets with a large and pronounced splitting. The model parameters, collected in table 4, are obtained by a least-squares fit using the nonlinear Levenberg–Marquardt algorithm. The procedure, however, is not entirely straightforward, due to the large number (~ 25) of parameters and possible correlations among some of them. To avoid local minima in the variational functional, corresponding to unphysical solutions, the algorithm is applied sequentially. In the initial steps, the relative energies and widths of the ansatz terms are kept fixed at their theoretical values and only the amplitudes are varied, so that a linear problem with a well defined single minimum is solved. In this way, the completeness of the ansatz is tested. The residual of the data, after subtracting the model, may show the presence of additional channels, as in the case of the 1s3d group. In the final steps, the widths and energy parameters are freed to vary one by one, to test their stability. The rationale of letting the widths vary is the fact that the model components describe a whole multiplet whereby their width can be increased over the lifetime value. The range of shake-off components is fixed at the 40% of the relative threshold energy as already mentioned.

Similarly, the restriction of energy parameters to their HF or DF values may be removed at the final stage of the analysis to allow for small adjustments since the effective centroids of the model components need not coincide with the DF multiplet averages. The 1s3s group, however, is treated more simply: the singlet–triplet splitting of ~ 6 eV is ignored in the model since the small signal-to-noise ratio makes only the separation of shake-up and shake-off statistically significant.

The agreement of the model energies with theoretical values depends on the relative energy of the coexcitation: the difference amounts to a few tenths of an electronvolt in valence coexcitations of table 1, and less than 2 eV in the deep MPE of table 4. The 5 eV difference of the 1s3s group has additional causes in the well known weak convergence of HF calculation for configurations with more than one open s subshell (three in 1s3s Rb!), and in the simple two-component model. It should be noted, however, that the accuracy of the energy parameter can directly be estimated only in the 1s3d group with a recognizable resonant component. In 1s3p and 1s3s groups with a predominant edge shape, the energy parameter of the model edge is not so sharply defined. The same apparent edge can be described with a model edge with an arbitrary shift upwards of the order of its width, if a resonance of an appropriate amplitude is inserted. In the same way, the threshold of a model shake-off component is correlated with the amplitude of the preceding model edge. In both cases, a meaningful value of amplitude is only obtained when the correlation is removed by fixing the relative energy at the theoretical value.

In this view, the parameters in table 4 represent minimal models sufficient to describe the MPE groups within experimental accuracy. In other words, we show that the MPE features

Table 4. Model parameters of the Kr and Rb 1s3d, 1s3p and 1s3s groups: (threshold) energies, widths/ranges and resonant intensities or shake amplitudes together with calculated energies (DF multiplet centres) of the corresponding electron transitions. Double values for the 1s3s group denote singlet–triplet splitting where a single model component is used. The estimated error of the amplitude parameters is one or two units of the last digit: the accuracy of the data in general is discussed in section 4.

Kr	Model				DF
	$E - E_K$ (eV)	Γ (eV)	$A\Gamma$ (10^{-2} eV)	A (10^{-2})	$E - E_K$ (eV)
[1s3d]4d5p	114	7	2.5		113
	118	6	0.7		116
[1s3d]4d	119	10		1.3	118
[1s3d]	126	50		0.6	124 ^a
[1s3d4p]4d ³	137	9	0.6		135 ^a
[1s3d4p]4d ²	143	10		0.1	137 ^a
[1s3d4p ²]4d ³ 5p	161	9	0.1		158 ^a
[1s3p _{3/2}]5p ²	242	7	0.5		244
[1s3p _{1/2}]5p ²	250	7	0.4		252
[1s3p _{3/2}]5p	246	7		0.1	247
[1s3p _{1/2}]5p	254	7		0.1	255
[1s3p _{3/2}]	252	100		0.3	254
[1s3p _{1/2}]	261	100		0.3	263
[1s3s]5s5p					317; 325
[1s3s]5s	313	9		0.02	320; 327
[1s3s]	323	130		0.07	331; 337
Rb					
[1s3d]4d5p	136	7	3.9		135
	142	4	0.7		140
[1s3d]4d	140	8		0.8	137
	145	4		0.2	147
[1s3d]	152	66		0.6	150
[1s3d4p]4d ³	163	9	0.4		160 ^a
[1s3d4p]4d ²	173	10		0.05	164 ^a
[1s3p _{3/2}]5p ²	270	7.0	0.4		275
[1s3p _{1/2}]5p ²	280	9.0	0.4		285
[1s3p _{3/2}]5p	274	6.5		0.1	279
[1s3p _{1/2}]5p	285	8		0.2	289
[1s3p _{3/2}]	283	115		0.3	287
[1s3p _{1/2}]	293			0.3	298
[1s3s]5s5p					352.8; 359.6
[1s3s]5s	358	9.0		0.04	356.9; 363.8
[1s3s]	370	148		0.05	368.5; 375.4

^a HF value.

can be explained as simple combinations of well known channels. The relevant results of the analysis are the best-fit amplitudes of the components; the energy and width parameters show the concordance with theoretical predictions. The estimated error of the amplitudes is one or two units of the last digit.

The model amplitudes in table 4 invite comparison with earlier Kr data. Among recent reports only Schaphorst *et al* [8] and Padežnik Gomilšek *et al* [26] include cross sections of separate channels. The latter use a similar approach to ours and report the 1s3d and 1s3p shake-up amplitudes as 1.4 and 0.3%, respectively, agreeing with our data to within experimental error. Schaphorst composed the models of MPE features from *ab initio* calculated cross sections and

demonstrated their fit with the experimental spectrum. His values of 1.4 and 0.2% for 1s3d and 1s3p shake-up, respectively, agree well with our results. The value of 3.7% for the 1s3d shake-off, however, is six times larger than ours. The fit of this calculated value with experimental data is only possible with an arbitrary choice of the baseline onto which the 1s3d feature is superposed. Since the curvature of the baseline is particularly large in this region, we feel that our exponential ansatz, taking into account the entire MPE region, produces a more reliable value for the shake-off amplitude. The 1s3p shake-off amplitude of 0.8% is again close to our value, conceivably due to the smaller curvature of the baseline beneath the 1s3p group.

There are no earlier data on atomic Rb absorption for comparison, but the presence of MPE in EXAFS spectra of Rb^+ ions in a solution has been demonstrated [48]. Recently, however, De Panfilis *et al* [49] have reported a measurement on molten Rb droplets: the spectrum shows all of the major MPE groups with a negligible contribution from the structural signal. The decomposition into principal excitation channels is indicated but no quantitative data are extracted.

In the present analysis the investigated spectral region has been wide enough, comprising several separate MPE groups, to attract attention to the increased slope above the edge and to show that its segments seen in the spaces between MPE groups resemble a single continuum. With a simple heuristic ansatz the entire spectrum is transformed into a more comprehensible form. We do not claim that the physics of virtual Auger excitations and PCI contribution is adequately represented: indeed, it is rather evident that the ansatz needs some local adaptation. The removal of a single exponential cannot flatten out all gaps between subshell groups: a larger decay constant would be needed for the region of 5s, 4p and 4s coexcitation groups, and a smaller one for the deep coexcitation. Evidence for some interference between this channel and the 3d coexcitation is given by the strong curvature of the cross section just below the 1s3d edge which escapes modelling with the standard ansatz. Nevertheless, the single exponential successfully removes the anomalous slope over the entire MPE region and over an order of magnitude. A considerably more precise measurement will be necessary to improve the ansatz with reliable additional terms.

5. Conclusions

The Rb vapour absorption experiment has provided the first instance of a comprehensive MPE spectrum outside the noble-gas group and has opened the way to comparison of MPE between neighbours. The advantage is twofold: the alkali spectra are less transparent due to the richer multiplet structure, so that the identification of features is considerably facilitated by the simpler structure of spectra of their noble-gas predecessors. On the other hand, the explanation of some ambiguous reaction channels in noble-gas spectra is aided by the evolution of the excitation scheme in the $Z + 1$ case.

The deconvolution of natural width in Kr and Rb has considerably improved the explanation of the edge region and of the strong valence MPE where the signal-to-noise ratio is still sufficiently high so that some expansion of noise can be tolerated in sharpening of the spectral features.

Together with the sharper view of the MPE features the PCI contribution is fully recognized in its span over the entire MPE region. A heuristic model is proposed in the absence of theoretical data. With the model, the photoabsorption cross section is reasonably transformed into a superposition of contributions of consecutive shake channels.

The unifying principle of the MPE spectra in both elements is the ground state CI: the admixture of the $[4p^2]4d^2$ configuration introduces strong additional channels in the three most prominent groups of MPE. The difference between the two elements is less striking: it

is epitomized by 5s coexcitations in the Rb edge region and by the specifically strong 5s–5p coupling. Another instance is the imminent 4d collapse. In many of these aspects, the Kr–Rb pair behaves in complete analogy with the Ar–K homologues. It is thus possible to introduce the concept of a noble-gas and/or alkaline MPE scheme.

Acknowledgments

Support of the Slovenian Ministry of Education, Science and Sport and of Internationales Büro des BMBF (Germany) is acknowledged. The experiment at the ESRF was performed under proposal no He-375; expert advice on BM29 beamline operation by A Filipponi and M Borowski is gratefully acknowledged, as well as the assistance of the former in the deconvolution procedures.

References

- [1] Deslattes D, LaVilla R E, Cowan P L and Henins A 1983 *Phys. Rev. A* **27** 923
- [2] Deutsch M, Maskil N and Drube W 1992 *Phys. Rev. A* **46** 3963
- [3] Deutsch M and Hart M 1986 *Phys. Rev. A* **34** 5168
- [4] Deutsch M and Hart M 1986 *Phys. Rev. Lett.* **57** 1566
- [5] Deutsch M and Hart M 1986 *J. Phys. B: At. Mol. Phys.* **19** L303
- [6] Bernieri E and Burattini E 1987 *Phys. Rev. A* **35** 3322
- [7] Ito Y, Nakamatsu H, Mukoyama T, Omote K, Yoshikado S, Takahashi M and Emura S 1992 *Phys. Rev. A* **46** 6083
- [8] Schaphorst S J, Kodre A, Ruscheinski J, Crasemann B, Åberg T, Tulkki J, Chen M H, Azuma Y and Brown G S 1993 *Phys. Rev. A* **47** 1953
- [9] Zhang K, Stern E A, Rehr J J and Ellis F 1991 *Phys. Rev. B* **44** 2030
- [10] Arčon I, Kodre A, Štuhec M, Glavič-Cindro D and Drube W 1995 *Phys. Rev. A* **51** 147
- [11] Deutsch M, Brill G and Kizler P 1991 *Phys. Rev. A* **43** 2591
- [12] Deutsch M and Kizler P 1992 *Phys. Rev. A* **45** 2112
- [13] Fano U and Cooper J W 1968 *Rev. Mod. Phys.* **40** 441
- [14] Sukhorukov V L, Hoppersky A N and Petrov I D 1991 *J. Physique II* **1** 501
- [15] Sukhorukov V L, Hoppersky A N, Petrov I D, Yavna V A and Demekhin V F 1987 *J. Physique* **48** 1677
- [16] Cooper J W 1988 *Phys. Rev. A* **38** 3417
- [17] Saha H P 1990 *Phys. Rev. A* **42** 6507
- [18] Štuhec M, Kodre A, Hribar M, Arčon I, Glavič-Cindro D and Drube W 1994 *Phys. Rev. A* **49** 3104
- [19] Deutsch M, Gang O, Hamalainen K and Kao C C 1996 *Phys. Rev. Lett.* **76** 2424
- [20] Fritsch M, Kao C C, Hamalainen K, Gang O, Foerster E and Deutsch M 1998 *Phys. Rev. A* **57** 1686
- [21] Armen G B, Åberg T, Karim K R, Levin J C, Crasemann B, Brown G S, Chen M H and Ice G E 1985 *Phys. Rev. Lett.* **54** 182
- [22] Kodre A, Arčon I, Hribar M, Štuhec M, Villain F and Parent P 1994 *J. Physique Coll. III* **4** C9 397
- [23] Chaboy J, Marcelli A and Tyson T A 1994 *Phys. Rev. B* **49** 11652
- [24] Kodre A, Arčon I, Hribar M, Štuhec M, Villain F, Drube W and Troeger L 1995 *Physica B* **208/209** 379
- [25] Solera J A, Garcia J and Proietti M G 1995 *Phys. Rev. B* **51** 2678
- [26] Padežnik Gomilšek J, Kodre A, Arčon I, Loireau-Lozac'h A M and Bénazeth S 1999 *Phys. Rev. A* **59** 3078
- [27] Padežnik Gomilšek J, Kodre A, Arčon I and Prešeren R 2001 *Phys. Rev. A* **64** 22508
- [28] Filipponi A and Di Cicco A 1995 *Phys. Rev. A* **52** 1072
- [29] Prešeren R, Kodre A, Arčon I, Padežnik Gomilšek J and Borowski M 2001 *J. Synchrotron Radiat.* **8** 279
- [30] Prešeren R, Arčon I, Mozetič M, Kodre A and Pregelj A 1996 *Nucl. Instrum. Methods B* **111** 161
- [31] Kodre A, Arčon I and Frahm R 1997 *J. Physique Coll. IV* **7** C2 195
- [32] Kodre A, Padežnik Gomilšek J, Arčon I and Prešeren R 1999 *J. Synchrotron Radiat.* **6** 306
- [33] Prešeren R and Kodre A 1999 *Radiat. Phys. Chem.* **55** 363
- [34] Filipponi A 2000 *J. Phys. B: At. Mol. Opt. Phys.* **33** 2835
- [35] Loeffen P W, Pettifer R F, Muellender S, van Veenendaal M A, Roehler J and Sivia D S 1996 *Phys. Rev. B* **54** 14877
- [36] Babanov Yu A, Ryazhkin A V and Sidorenko A F 1997 *J. Physique Coll. IV* **7** C2 277

- [37] Babanov Yu A, Ryazhkin A V, Sidorenko A F and Blaginina L A 1998 *Nucl. Instrum. Methods A* **405** 378
- [38] Breining M, Chen M H, Ice G E, Parente F and Craseman B 1980 *Phys. Rev. A* **22** 520
- [39] Dylla K G, Grant I P, Johnson C T, Parpia F A and Plummer E P 1989 *Comput. Phys. Commun.* **55** 425
- [40] Tulkki J and Åberg 1985 *J. Phys. B: At. Mol. Phys.* **18** L489
- [41] Amusia M Y, Ivanov V K and Kupchenko V A 1981 *J. Phys. B: At. Mol. Phys.* **14** L667
- [42] Teodorescu C M, Karnatak R C, Esteva J M, El Afif A and Connerade J-P 1993 *J. Phys. B: At. Mol. Opt. Phys.* **26** 4019
- [43] Prešeren R 2000 *Dissertation* Faculty of Mathematics and Physics, Ljubljana
- [44] Krause M O and Oliver J H 1979 *J. Phys. Chem. Ref. Data* **8** 329
- [45] Froese Fischer C 1987 *Comput. Phys. Commun.* **43** 355
- [46] Dylla K G 1983 *J. Phys. B: At. Mol. Phys.* **16** 3137
- [47] Arčon I and Kodre A 1997 *J. Physique Coll. IV* **7** C2 233
- [48] D'Angelo P, Di Nola A, Giglio E, Magnoni M and Pavel N V 1995 *J. Phys. Chem.* **99** 5471
- [49] De Panfilis S, Di Cicco A, Filipponi A, Comez L and Borowski M 2001 *J. Synchrotron Radiat.* **8** 764